Upstream basin circulation of rotating, hydraulically controlled flows

Adele Morrison

Australian National University

August 18, 2012

1 Introduction

1.1 Motivation

The overflows of dense water from the Nordic Seas into the North Atlantic are a key element of the global meridional overturning circulation. The deep southward limb of the overturning is fed primarily by the overflows, and the transport of the deep limb is closely linked to the transport in the warmer northward currents in the upper ocean of the North Atlantic. The threat of potentially significant shifts in climate due to changes in the overturning motivates an improved understanding of the overflows and the associated upstream basin circulation. Despite enhanced recent efforts [1, 2], the source regions and pathways of the deep water masses upstream of the overflows remain uncertain.

Observations of the Denmark Strait and Faroe Bank Channel, the two primary exit points of deep water from the Nordic Seas, indicate that the overflows are hydraulically controlled. Hydraulic control is qualitatively suggested by the characteristic spillage observed in the drawdown of downstream isopycnals (Figure 1), the lack of seasonality in overflow transport
and the dependence of the overflow transport on upstream interfacial elevation. The hydraulic control has also been quantitively confirmed by the identification of control sections where the flow undergoes sub-critical to super-critical transitions [4].

A feature of hydraulically controlled flows is that the stratification in the basin upstream of the overflow sill or strait consists of a uniform dense layer overlaid by a dynamically inactive upper layer, as shown in Figure 1. It is therefore not unreasonable to model the upstream basin as a single fluid layer (or $1\frac{1}{2}$ layers with reduced gravity) governed by the shallow water equations.

Here we focus on the nature of the upstream basin circulation in an idealised one layer model with circular basin geometry and varying source location, using a combination of laboratory and numerical experiments.

1.2 Overview

Monitoring the transport of the Nordic Sea overflows has long been a goal of the oceanographic community. Direct current measurements are difficult due to the complex structure
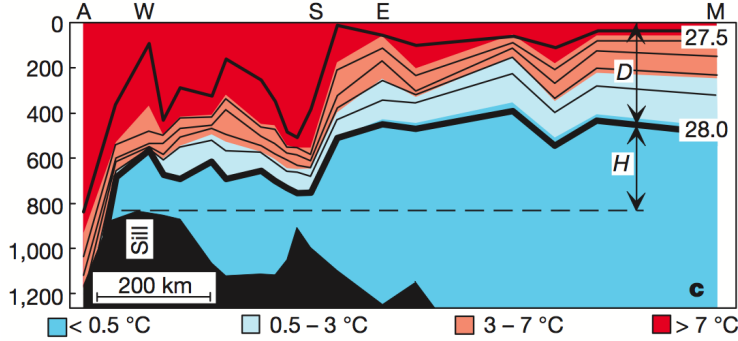
1

Figure 1: An along-stream section of the Faroe Bank Channel indicating the characteristic spillage of hydraulically controlled flows, showing temperature (colour shading) and isopycnals (contours). From Hansen et al. (2001)[3].

of the flows. Instead, observational studies have attempted to infer overflow transports from upstream hydrographic measurements [3, 5], as suggested may be reasonable by the rotating hydraulic theory of Gill [6]. Calculation of the overflow transport using Gill's theory, which assumes a uniform potential vorticity flow through a rectangular cross-section channel, requires knowledge of the upstream basin circulation (ie. interfacial height on a boundary), as well as the strait geometry and potential vorticity. On the contrary, Helfrich and Pratt (2003)[7] have shown that the overflow transport in an idealised numerical model depends only on the strait parameters (geometry and potential vorticity) and not the upstream circulation. The simulated basin-strait system selects the Gill solution with maximum potential energy in the basin. This implies that accurate estimates of the transport cannot be gained from upstream information. The original plan for this project was to perform an experimental comparison of the findings of Helfrich and Pratt (2003). However, we were unable to pursue this question very far due to limitations of the experimental parameter range. In particular, the width of the strait in the experiment was small compared with the Rossby radius, placing it in a different regime from the previous numerics.

As an alternative, we have focused on the dependence of the circulation direction in the upstream basin on the potential vorticity flux through the basin, as introduced in Section 1.3. We show that, for the parameter regime of the experiments, the relative vorticity component of the potential vorticity flux cannot be ignored and that the commonly assumed simple dependence of the flow direction on the relative thicknesses of the inflow and outflow does not necessarily hold for hydraulic flows.

1.3   Potential vorticity balance of the upstream basin circulation

Previous studies of boundary layer flows in semi-enclosed basins have shown that the direction of circulation (ie. cyclonic or anticyclonic) in the basin is strongly dependent on the potential vorticity (PV) fluxes at the inflow and outflow [7, 8, 9]. Integrating the PV over the entire basin yields a balance between the net PV fluxed in or out of the basin and the dissipation of PV by friction. Here we derive the PV balance, following Yang and Price

(2000) [10]. We begin with the shallow water momentum and continuity equations:

$$\frac{Du}{Dt} - fv + g\frac{\partial h}{\partial x} = -\lambda u \tag{1}$$

$$\frac{Dv}{Dt} + fu + g\frac{\partial h}{\partial y} = -\lambda v \tag{2}$$

$$\frac{Dh}{Dt} + h\left(\frac{\partial u}{\partial x} + \frac{\partial v}{\partial y}\right) = 0, \tag{3}$$

where $\frac{D}{Dt}$ is the material derivative, (u, v) are the velocity components, h is the layer depth, f is the Coriolis parameter and λ is the Rayleigh bottom friction coefficient. Given the northerly latitude and small size of the basins under consideration, we take f to be constant. The vorticity equation may be obtained by taking the curl of the momentum equations:

$$\frac{\partial}{\partial t}(\nabla \times \mathbf{u}) + \nabla \times ((f + \nabla \times \mathbf{u}) \times \mathbf{u}) = -\lambda \nabla \times \mathbf{u}. \tag{4}$$

Extracting the steady state, vertical component of the vorticity equation (applying incompressibility and noting that the divergence of the vorticity is zero) gives:

$$(\mathbf{u} \cdot \nabla)(f + \zeta) = (f + \zeta)\frac{\partial w}{\partial z} - \lambda \zeta \tag{5}$$

where $\zeta = v_x - u_y$ is the vertical component of the relative vorticity and w is the vertical component of the velocity. Rearranging the term on the left (again using incompressibility and separating the divergence into horizontal and vertical parts), we obtain:

$$\nabla \cdot [\mathbf{u_h}(f + \zeta)] + \frac{\partial}{\partial z}[w(f + \zeta)] = (f + \zeta)\frac{\partial w}{\partial z} - \lambda \zeta \tag{6}$$

where $\mathbf{u_h} = (u, v)$ is the horizontal vorticity. The second and third terms in this equation are similar in form. The term $\frac{\partial}{\partial z}[w(f + \zeta)]$ represents vorticity transport due to a vertical mass flux into the layer, while $(f + \zeta)\frac{\partial w}{\partial z}$ is the usual vortex stretching term. If adjacent layers have different relative vorticity (ie. $\frac{\partial \zeta}{\partial z} \neq 0$), there is not necessarily a cancellation between the two terms. For downwelling located in the interior of a basin, the upper layer flow will likely be slow and geostrophic, and thus $f \gg \zeta$ is a reasonable assumption. However this is not necessarily the case for downwelling near a basin boundary (within a boundary layer flow). Given this caveat, Yang and Price [10] make the assumption that $f \gg \zeta$, which reduces Equation 6 to:

$$\nabla \cdot [\mathbf{u_h}(f + \zeta)] = -\lambda \zeta \tag{7}$$

Under the shallow water approximation, all variables are assumed to be depth independent, allowing us to rewrite Equation 7 in terms of depth-integrated variables:

$$\nabla \cdot \left[\mathbf{U_h}\left(\frac{f + \zeta}{h}\right)\right] = -\lambda \zeta, \tag{8}$$

where $\mathbf{U_h} = \mathbf{u_h}h$ is the depth integrated horizontal velocity and $\frac{\zeta + f}{h}$ is the potential vorticity. Finally, integrating Equation 8 over the entire basin and applying the divergence and

Stokes theorems, we obtain a balance between the net PV fluxed in or out of the basin and the dissipation of PV by friction:

$$\oint_C (\mathbf{U_h} \cdot \hat{\mathbf{n}}) \left(\frac{f + \zeta}{h} \right) ds = -\lambda \oint_C \left(\mathbf{u_h} \cdot \hat{\mathbf{t}} \right) ds \tag{9}$$

where C is the boundary of the basin, $\hat{\mathbf{n}}$ is the normal vector across the basin boundary and $\hat{\mathbf{t}}$ is the tangential vector along the boundary. The term on the left of Equation 9 is simply the net PV fluxed out of the basin via the open boundaries at the inflow and outflow, ie.

$$Q \left[\left(\frac{f + \zeta_{out}}{h_{out}} \right) - \left(\frac{f + \zeta_{in}}{h_{in}} \right) \right] = -\lambda \oint_C \left(\mathbf{u_h} \cdot \hat{\mathbf{t}} \right) ds. \tag{10}$$

Equation 10 implies that if the net PV flux through the openings is positive, the average direction of the circulation on the basin boundary must be anticyclonic, so that the dissipation of PV balances the net flux. Similarly, if the net PV flux is negative, the average boundary circulation direction is cyclonic. Yang and Price (2000) [10] simplify this balance even further, by assuming a 'slug' (unidirectional and steady) flow at both the inflow and outflow to argue that the relative vorticity integrated across an opening must be zero. The relative vorticity component will also vanish in a model with no-slip conditions. This assumption leads to:

$$Q f \left[\left(\frac{1}{h_{out}} \right) - \left(\frac{1}{h_{in}} \right) \right] = -\lambda \oint_C \left(\mathbf{u_h} \cdot \hat{\mathbf{t}} \right) ds. \tag{11}$$

Numerical simulations of Yang and Price (2000) [10] and Yang (2005) [9], using a free-slip boundary to determine the dissipation given by the circulation integral, and prescribed, uni-directional flows at the openings (so that the simplification of Equation 11 holds), show that by changing the relative heights of the inflow and outflow (and therefore the sign of the net PV flux), the circulation can be made to switch direction in the basin, as shown in Figure 2. For a net PV flux of zero, the inflow was found to split into two branches, so that the circulation direction differed across the two sides of the basin. This relation between the net PV flux and the direction of basin circulation has been used to explain the puzzling discrepancy of the circulation direction in the models of the Arctic Ocean Model Intercomparison Project [9].

Although the dependence of the circulation direction given by Equation 10 relies strongly on the linear friction parameterisation, numerical studies using smaller frictional coefficients, no-slip boundary conditions or lateral friction instead of bottom friction have also found consistency between the sign of the PV flux through the basin and the circulation direction [9, 10].

1.4 Review of previous studies of upstream basin flows

In this section, we review past numerical, analytical and experimental studies, which have examined the structure of the flows in basins upstream of a hydraulically controlled sill.

Pratt (1997)[8] derived analytical expressions for the boundary layer currents that link the upstream sources to the overflow strait. The flows are equivalent to the northern or southern boundary layers arising in a homogeneous Stommel circulation in a rectangular
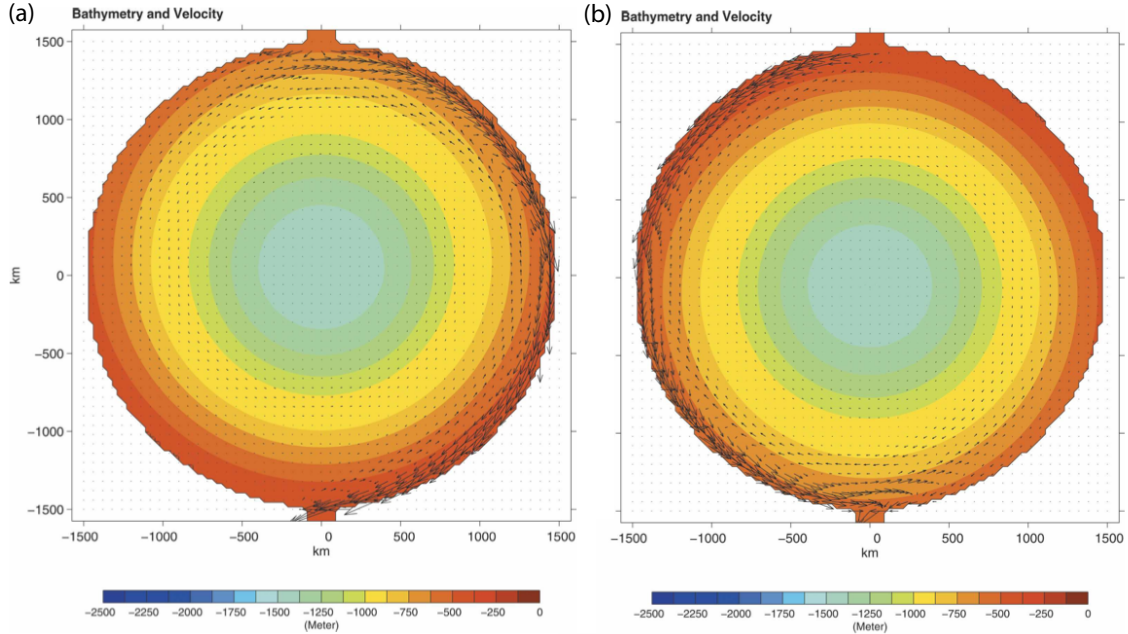
Figure 2: Numerical simulations showing the control of the net PV flux through the basin on the circulation direction. The left figure (a) shows the case where the PV flux at the outflow is larger than the inflow, which was achieved by tilting the basin such that $h_{out} < h_{in}$. The right figure (b) shows the effect of tilting the basin in the opposite direction. From Yang (2005) [9].

basin. Variation in topographic slope near the boundary replaces the latitudinal variation of f. An average estimate of the boundary layer thickness, δ, arises from what is essentially a diffusion equation with angle around the basin replacing the role of time:

$$\delta = \sqrt{R_b}\sqrt{\frac{\lambda}{\beta_T}} \tag{12}$$

where R_b is the basin radius, $\beta_T = -f\frac{\partial}{\partial r}\left(\frac{h}{H_o}\right)$ is the topographic beta and H_o is the depth scale. The diffusive nature of the solution gives rise to a spreading of the boundary layer as the current flows from the inflow source to the exit strait. Pratt matched this solution to various inflow and outflow boundary conditions and found that all of the analysed solutions have the flow entering the strait along the left wall (note we will use 'left' and 'right' as if looking downstream from the basin towards the overflow channel). The left wall may be interpreted as a western boundary with the beta effect arising due to the presence of a topographic slope between the basin and strait. The solution for a source located on the boundary opposite the outflow channel has two opposing boundary layers, as shown in Figure 3. The boundary layer along the right wall overshoots the strait to join the left wall boundary layer and enter the strait from the left. Note that the inflow was assumed to split in order to feed the two boundary layers directly.
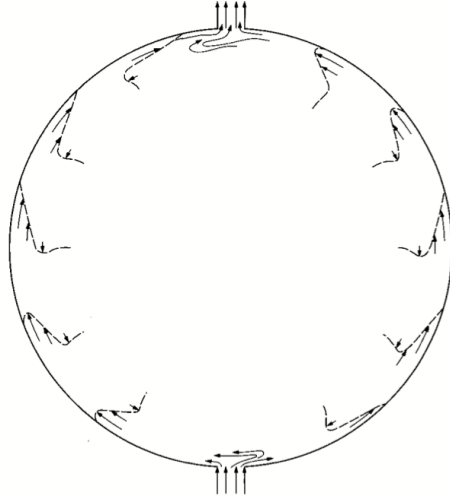
5

Figure 3: Analytical boundary layer solution of Pratt (1997)[8] for basin flow fed by an isolated boundary source and sink.

The primary experimental study that has looked at the nature of the flows upstream of a controlling passage was that of Whitehead and Salzig (2001)[11]. This study observed the qualitative features of the upstream circulation for varying source locations. For all source locations, Whitehead and Salzig observed the current entering the strait from the left, either flowing directly along the left wall or overshooting the strait from the right wall to enter along the left. For a source located on the right hand boundary wall upstream of the strait, the flow formed a boundary layer on the right wall which crossed to the left side of the strait entrance before forming a tightly curving current on the left wall of the exit strait. Fluid entering through a source on the left boundary, just upstream of the channel, was observed to flow directly along the left wall to the overflow channel. A source placed in the centre of the upstream basin formed a clockwise boundary current around the edge of the basin.

Helfrich and Pratt (2003)[7] investigated upstream flows in numerical simulations using two different source locations. A uniform downwelling over the entire basin created a domed interface and an essentially geostrophic, anticyclonic circulation, with fluid approaching the strait along the left wall. With an inflow on the boundary directly opposite the strait, the flow split into two boundary currents, which rejoined at the strait. An asymmetry was observed between the two currents, with the right wall current stronger and overshooting the strait to enter from the left.

2 Laboratory experiments

2.1 Apparatus and procedure

The experiments were carried out in a basin on a 1 m diameter rotating table in the geophysical fluid dynamics laboratory at the Woods Hole Oceanographic Institution, as

6

depicted in Figure 4. The parabolic basin had a depth of 0.20 m and a radius of 0.46 m. A vertical sidewall of height 0.10 m was attached to the top of the basin edge following the curvature of the basin, except near the side inflow and outflow strait, where the radius of curvature was 0.12 m and 0.20 m respectively, in order to smoothly connect the inflow and outflow channels. For all but one experiment, the overflow sill had a height of 0.025 m and was positioned within the outflow strait, which had a width of 0.13 m, at a distance of 0.20 m from the basin edge.
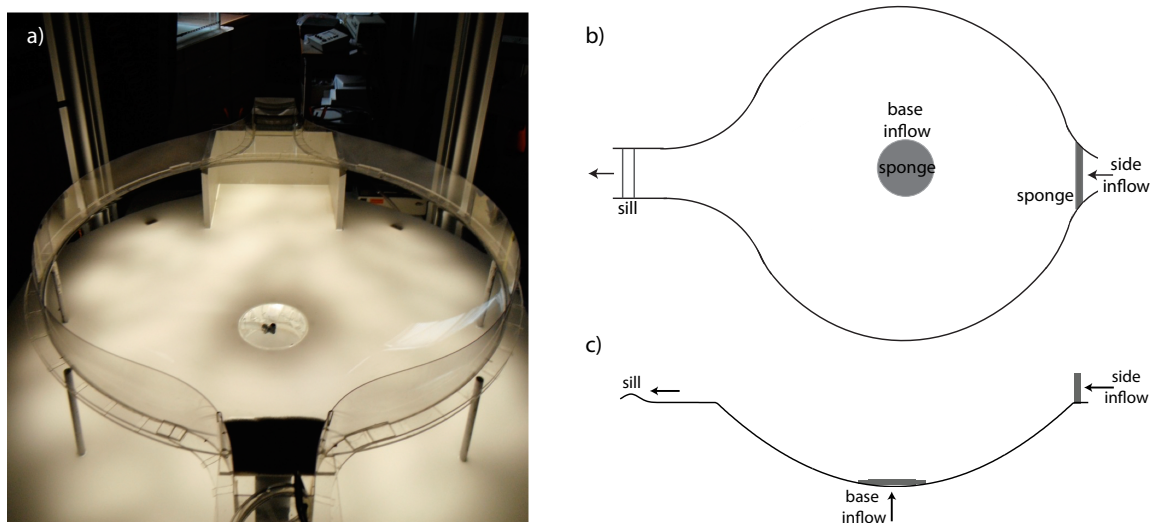
Figure 4: The experimental apparatus, shown from a,b) top view and c) side view.

The inflow location was varied between a boundary and centred upwelling region. For the boundary inflow, water entered the basin directly opposite the strait, through a sponge which had a width of 0.12 m and was aligned with the basin edge. For the case of upwelling inflow, water entered through a circular sponge of radius 0.07 m at the bottom of the tank. The overflow water was collected in a basin, before being pumped back to the inflow. Pump rates varied between $(10 - 40)$ mL/s $((0.77 - 3.08) \times 10^{-4}$ m^3/s$)$ and the basin was rotated anti-clockwise with a range of rotation rates corresponding to $f = (1, 1.5, 2)$ s^{-1}.

A lid was fitted on top of the entire basin during all experiments in order to reduce the effects of surface stress from the overlying air. The basin was lit from below using ~ 300 white LEDs below a diffuser. With the table rotating and the pump switched on, the basin was left to spinup for 30 minutes. Dye was then released into the inflow at a constant rate of $\sim$15 mL/hr. At higher dye release rates, the interface between the central undyed fluid and the dyed right wall current was observed to tilt and become baroclinically unstable. The advection of dye by the flow was imaged from above by a co-rotating black and white camera, with images taken at intervals of 0.5 s.

Using the same scaling for the channel depth h_o as Whitehead and Salzig (2001) [11], gives a Rossby radius $(R_d = \sqrt{gh_o}/f)$ in the range of $(0.2 - 0.4)$ m for the range of experimental parameters. The strait width is therefore much less than the Rossby radius and the hydraulic control on the basin will be more similar to the non-rotating case.

Due to the brief nature of the summer project, it was decided not to perform quantitative measures of the circulation, such as particle image velocimetry (PIV), at this time.

2.2 Qualitative description of the flows

The flow behaviour observed in the experiments qualitatively agrees with the expected flows from previous numerical simulations [7, 9] and a theoretical boundary layer solution [8], as described in Section 1.4, except that the case of boundary inflow is rarely (if ever) observed to split into a left wall and right wall current, as described in these previous studies.

2.2.1 Boundary inflow

Figure 5 shows the progress of dye around the basin from the inflow to the strait. The dye was released at a constant rate into the inflow after the circulation had reached steady state. The inflow is entirely deflected to the right, into the cyclonic boundary layer. The cyclonic right wall current overshoots the strait, as also observed in previous numerics and experiments [7, 11]. The overshooting behaviour is a result of the flow looping back to form a nominal 'western' boundary current as it crosses background PV contours on the way out of the basin. Also seen in Figure 5c,d is a strip of undyed fluid exiting in the centre of the strait. This undyed fluid is fed from the anticyclonic left wall current, which spirals out of the centre of the basin. Given sufficient time, the overshooting right wall current would spiral inwards to the centre of the basin to eventually feed the outward spiralling left wall current. Similar circulation patterns were observed over a range of inflow fluxes and rotation rates.

Over the range of experimental parameters investigated (perhaps with the exception of the raised sill, discussed below), the inflow was not observed to split into a left wall and a right wall current, as was assumed in the interpretation of both the numerical simulations of Yang (2005) [9] and the analytical solution of Pratt (1997) [8]. In hindsight, reexamining these studies shows that the inflow (except perhaps for the case shown in Figure 2a) turns entirely to the right and that the left wall current is fed from the interior of the basin, rather than directly from the inflow.

The separation of the current from the left wall of the exit strait is due to the surface curvature resulting from the centripetal effect of the rotating table. The free surface height increases by an amount $d = \frac{\Omega^2 r^2}{2g}$ where $\Omega = f/2$ and r is the distance from the axis of rotation. For $f = 1$ s^{-1}, the surface is raised by 2.6 mm at the edge of the basin. For $f = 2$ s^{-1}, the effect becomes more significant with the surface raised by 10.6 mm. At higher rotation rates, the gradient of the thickness in the strait increases, resulting in an effective western boundary layer on the right wall of the strait.

2.2.2 Upwelling inflow

The experiments with a central upwelling source behaved much as expected from previous numerical work, with a predominantly anticyclonic geostrophic circulation. Figure 6 shows the steady state flow for a typical experiment. Dye enters the basin through the sponge at the center of the tank and gradually spirals outwards in the small ageostrophic component of the flow due to bottom friction. The boundary current around the rim of the basin
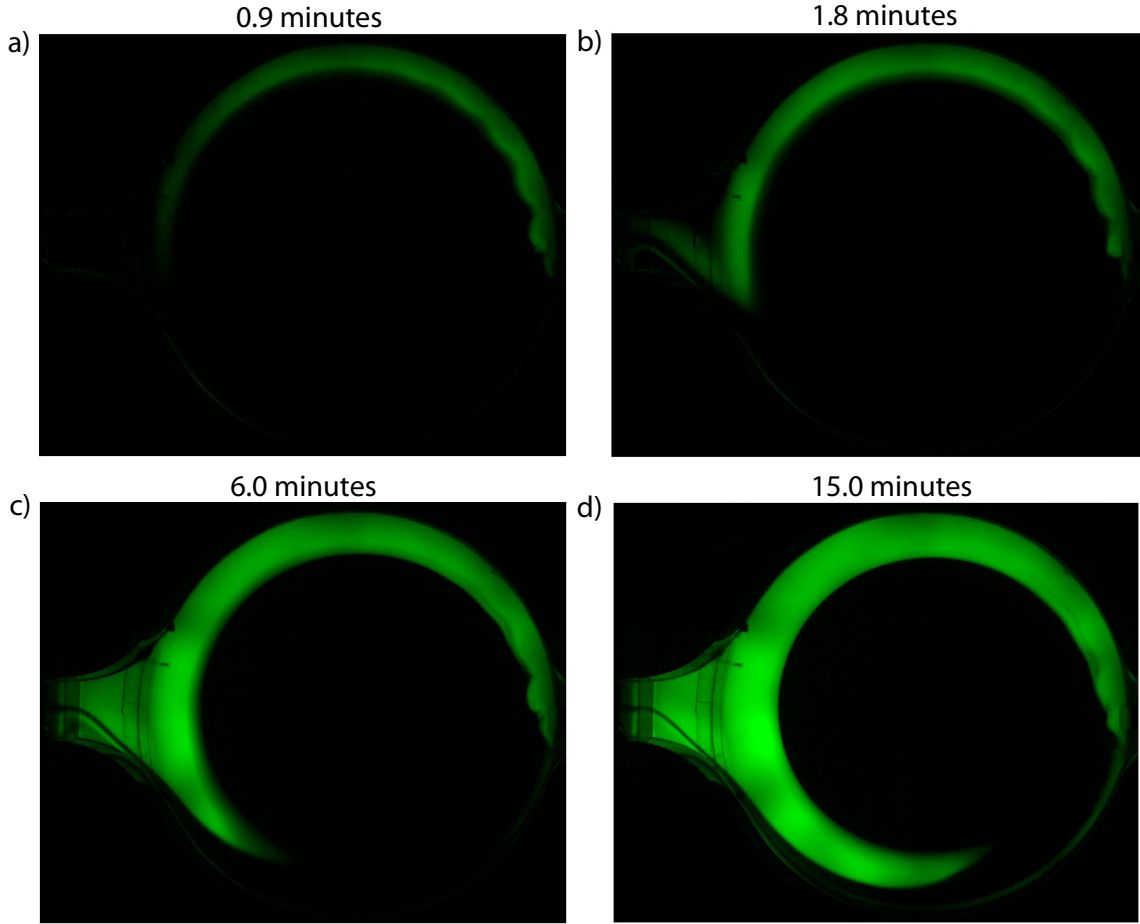
Figure 5: A sequence of false-colour photographs from the experiment showing the progression of dye around the basin. The inflow is on the right and strait on the left. The inflow was set to 30 mL/s and the rotation rate was $f = 1.5$ s^{-1}.

recirculates as well as feeding the overflow. A persistent feature of the flow is a cyclonic eddy at the entrance to the strait.

2.2.3 Raised sill

To investigate the dependence of the circulation direction on the PV budget, an experiment was carried out with a raised sill, of height 0.045 m. Apart from the location of the sill, the experimental parameters were identical to those of the experiment shown in Figure 5. The sill was placed at the edge of the basin to remove the effects of the strait on the circulation. It should be noted that the topographic gradient leading up to the sill was large. With a raised sill, the net PV flux through the boundary (under Yang's assumption that we can ignore the relative vorticity component) is strongly positive. According to the balance between the net PV flux and PV dissipation (Section 1.3) and the numerical simulations of
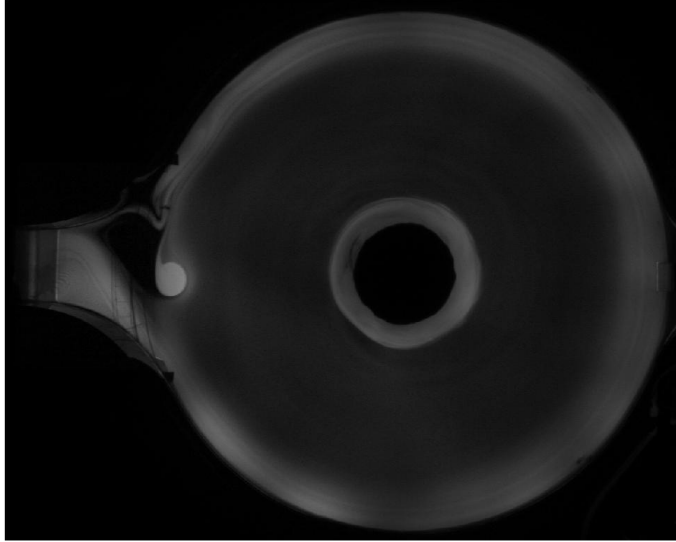
Figure 6: False-colour dye image for upwelling inflow through the base of the tank (through the dark patch in the centre). The inflow spirals anticyclonically outwards. Note the concentration of dye in the cyclonic eddy near the entrance to the strait. The inflow was set to 20 mL/s and the rotation rate was $f = 1.5$ s^{-1}.

Yang (2005) (Figure 2), we would expect the right wall current to be severely diminished (if present at all) and the circulation in the basin to be predominantly anticyclonic.

Figure 7 shows a timeseries of dye entering through the inflow. Compared to the experiment with a lower sill, the left wall current is noticeably stronger. It is unclear if the inflow is splitting into two directions, or if the left wall current is entraining dye from the right wall current as it spirals outwards from the centre of the basin. Despite the increased presence of the left wall current, the right wall current remains dominant and the circulation appears predominantly cyclonic. In order for the flow to satisfy the PV balance, either the relative vorticity components of the PV flux through the boundary must be significant, or dissipation along the left wall leading up to the strait dominates, despite the opposing contribution from the dissipation along the right wall.

3 Numerical simulations

3.1 Methods

Numerical solutions of the shallow water equations were computed in order to gain a more quantitative understanding of the flows seen in the laboratory. The model domain was constructed to closely mimic the experiments. Figure 8 shows the bathymetry, using rectangular cells with a resolution of 0.5 cm. The numerical model (described in detail in [12, 7]) solves the shallow water equations in flux form and using a second-order finite-volume method to allow shocks, hydraulic jumps and layer depths approaching zero, as are
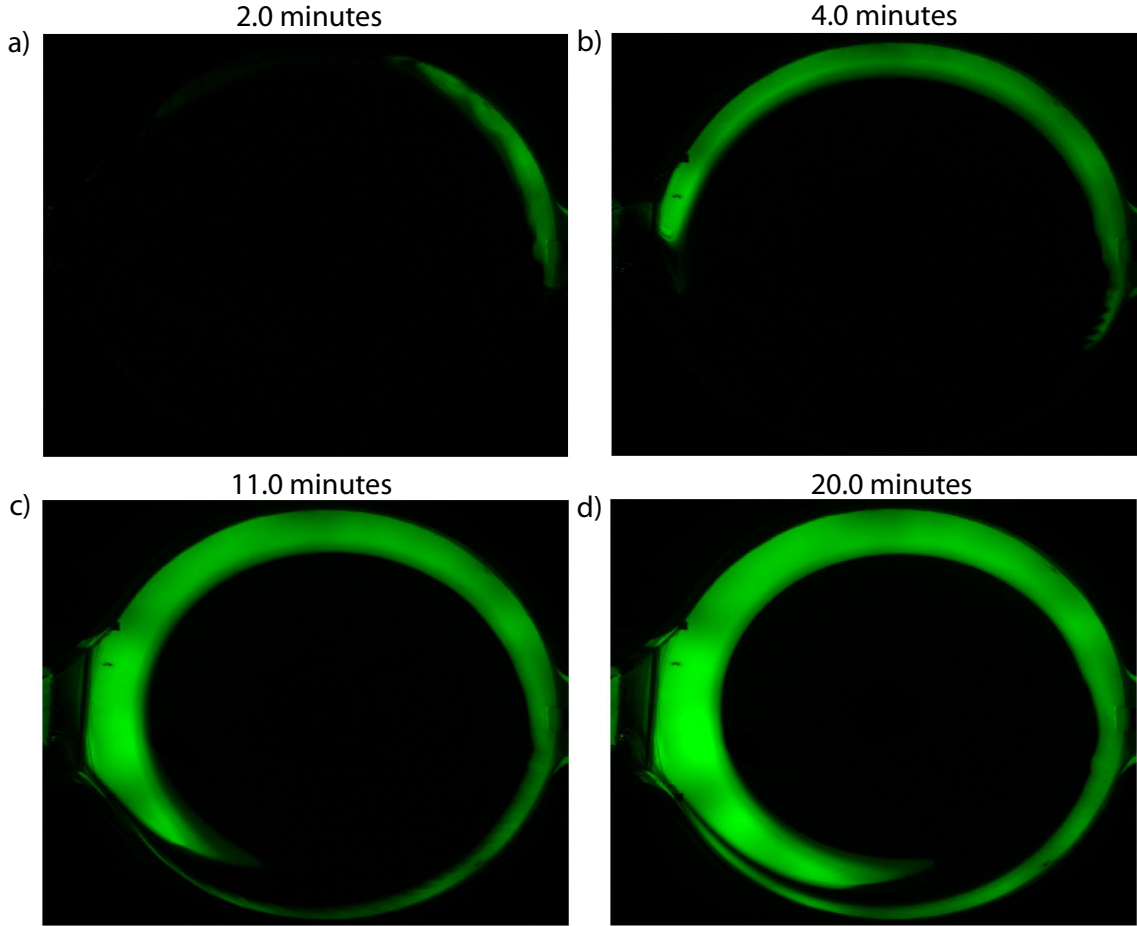
Figure 7: A sequence of photographs from the experiment with a raised sill. Apart from the location and height of the sill, the parameters were identical to the experiment shown in Figure 5. Note that the view of the strait is obstructed by the placement of the sill at the edge of the basin. The strength of the anticyclonic left wall current noticeably increases when the thickness of the outflow is reduced, though the right wall current remains dominant.

common in rotating hydraulics. The model was run out to equilibrium and a time mean used for the analysis described in the following sections.

3.2 Simulations of the experiments

The simulations described in this section had a no-slip boundary condition, small lateral friction, bottom friction and an added centripetal term to obtain the variation in free surface height seen in the experiments. The numerics reproduced the mean state of the experiments well. Figure 9 shows the mean state of the basin circulation with inflow through the side wall and with parameters typical of the experiments. The structure of the circulation is
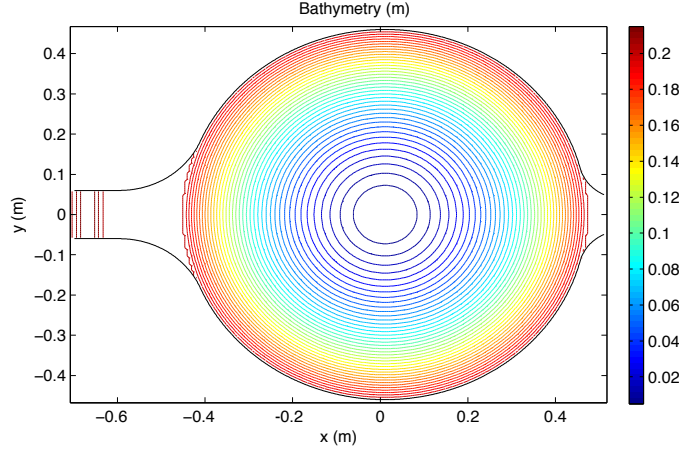
Figure 8: Bathymetry used in the numerical simulations.

remarkably similar to that observed in the experiments (Figure 5) and highlights the spiral structure of the flows, with the left wall boundary current spiralling anticyclonically out from the centre, while the overshooting right wall boundary current spirals cyclonically into the centre of the basin. The simulations show clearly that the left wall current in this case is fed from the interior of the basin, rather than from a direct splitting of the inflow, as was assumed for the flows in [8, 9].
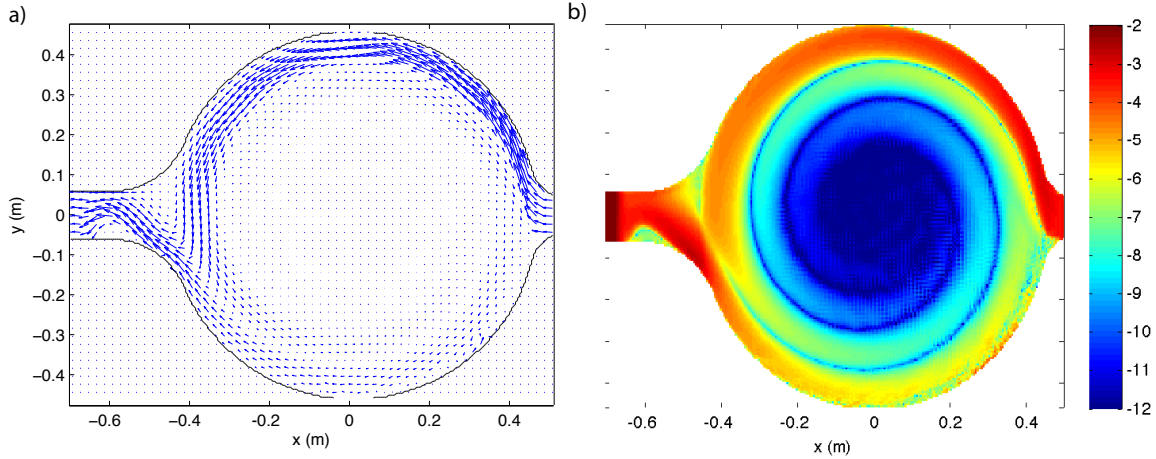
Figure 9: Time averaged numerical simulation of an experiment with side inflow $= 40$ mL/s and $f = 2$ s^{-1}. a) Velocity flow field at equilibrium. b) The log of the velocity magnitude.

The effect of adding the centripetal term $(\Omega^2 r)$ to the shallow water momentum equation is shown in Figure 10. The simulations demonstrate that the separation of the flow from the left wall of the strait, such as seen in Figure 5d, is a result of the enhanced thickness gradient due to the increased surface curvature that is present with the centripetal term.
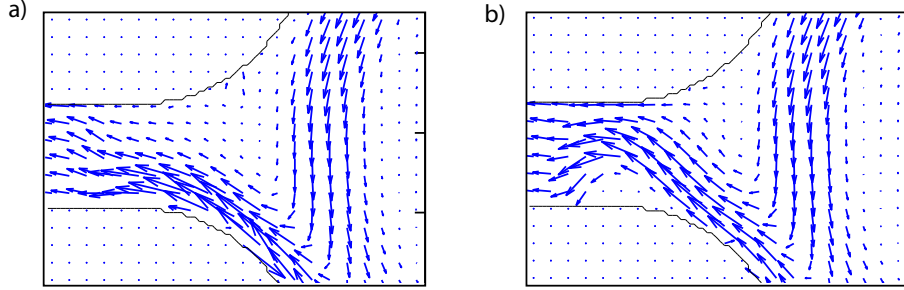
Figure 10: The effect of the centripetal term on the strait flow. Centripetal term switched a) off, and b) on.

The numerical simulations with inflow through the bottom of the basin are shown in Figure 11. Again, the features seen in the experiment, such as the anticyclonic geostrophic flow and the dominant eddy near the strait are also observed in the numerics.
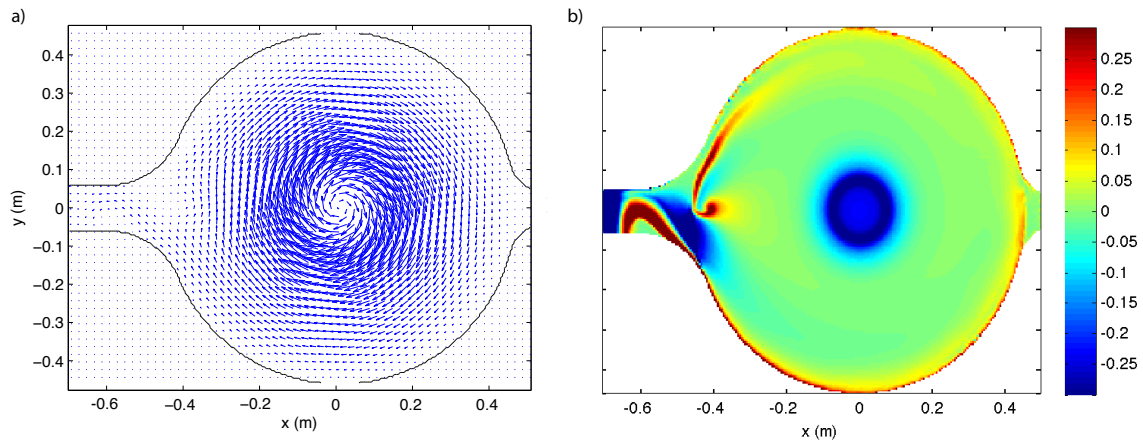

Figure 11: Numerical simulation of an experiment with bottom upwelling inflow $= 40$ mL/s and $f = 2$ s^{-1}. a) Time-averaged flow field at equilibrium. b) Relative vorticity.

3.3   Potential vorticity balance

A range of simulations with varying sill height were carried out to investigate the extent of the dependence of the basin circulation direction on the PV flux through the basin. These simulations were performed with free-slip boundary conditions and zero lateral friction, leading to the simple PV balance of Equation 10. As outlined in Section 1.3, as the height of the sill is raised, we would expect the net PV flux out of the basin to increase and therefore the dissipation should compensate by switching the direction of the flow, so that the inflow feeds the left wall boundary current (ie. the reverse of the flow shown in Figure 9).

Figure 12 shows the effect of doubling the sill height on the basin circulation. The right

wall boundary current weakens as the sill height is increased, but there is no clear switch in direction, as was expected. Alternatives for the flow to satisfy the PV balance without changing the direction of circulation may be either an increase in dissipation on the left wall, relative to the right wall, as the flow approaches the strait, or compensation by significant relative vorticity fluxes through the openings (previously assumed to be negligible). It seems unlikely that the former is the case, as the left wall boundary current also weakens and breaks up with increasing sill height. It is also apparent here that the jagged boundaries caused by the rectangular grid cells result in anomalies in the weak left wall boundary flows. In order to investigate if the relative vorticity fluxes are significant, the PV flux at the outflow was split into planetary and relative vorticity components, as shown in Figure 13 for varying sill height.
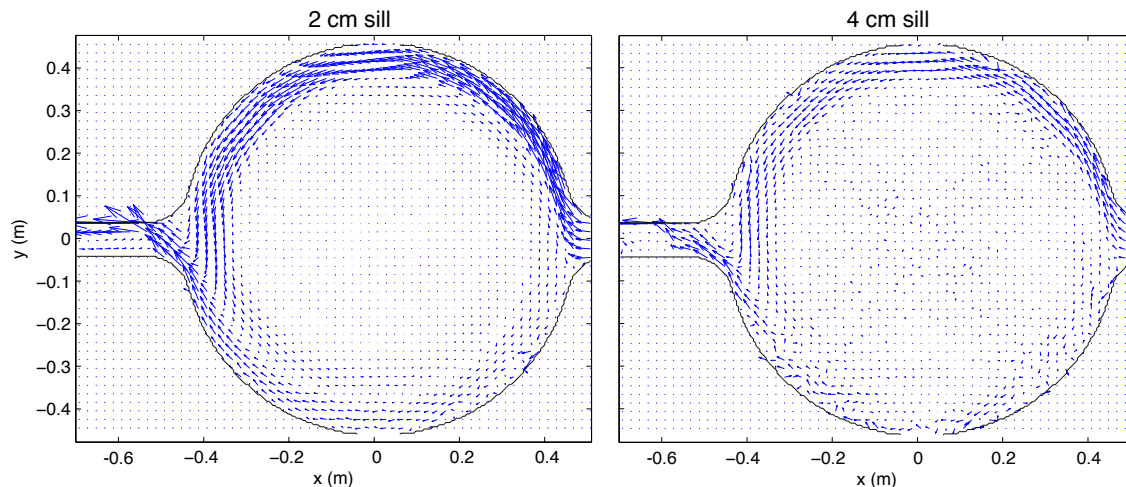

Figure 12: Comparison of simulations with varying sill height. The left (right) figure shows the flow for a 2 cm (4 cm) sill.

As the sill height is increased, the outflow layer thins, resulting in an increase in the planetary vorticity. The relative vorticity at the outflow compensates by becoming increasingly negative. Interestingly, the sum of the two vorticity components (ie. the net outflow PV) remains constant as the sill height is varied. Compared with previous work [8, 10, 9], these results show that, at least for the parameter range of the experiments, changes in the outflow planetary vorticity, resulting from changing fluid thickness, may be compensated by changes in relative vorticity at the outflow, rather than changes in basin dissipation (ie. a change in circulation direction). The primary difference between these numerical simulations and those of Yang (2005) is that we have not fixed the direction or transport of the flow at the exit of the basin. The compensation depicted in Figure 13 may be due simply to the freedom allowed for the flow to adjust, or perhaps a result of the criticality of the flow at the exit sill. It is possible that the relative vorticity at the North Atlantic overflows is insignificant, as is commonly assumed, and that our experiments and simulations are in a different parameter range. Figure 14 shows that we also see significant relative vorticity fluxes over a wider range of parameters (varying rotation rate, f, and transport, Q).
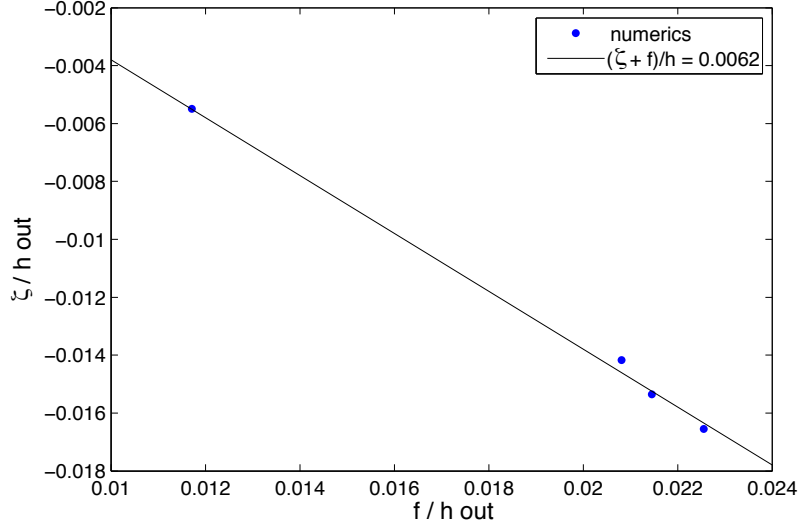
Figure 13: Variation of the relative versus planetary components of the potential vorticity flux at the outflow for changing sill height. Sill height increases towards the right of the figure. The line represents constant net potential vorticity at the outflow.

However in order to have a closer comparison with the real ocean, rotation rates roughly double these are required. The largest rotation rate $(f = 3 \text{ s}^{-1})$ of the simulations shown in Figure 14 corresponds to a Rossby radius equal to the width of the exit channel.
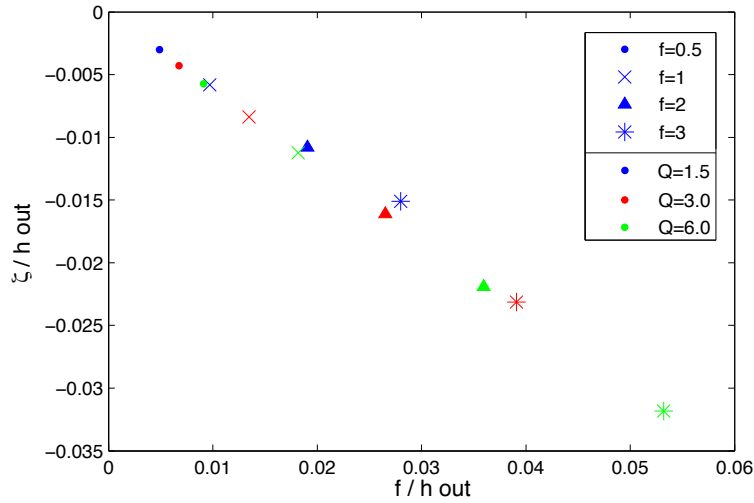

Figure 14: Variation of the relative versus planetary components of the potential vorticity flux at the outflow for a range of simulations with varying Coriolis parameter f and outflow transport Q.

The one caveat to these results is that we have had some difficulty in closing the PV budget of the basin. We expect this is due to the noisy boundary dissipation in the regions of low flow, as shown in Figure 15. Simulations run at double the resolution have significantly reduced boundary noise and improved closure of the PV budget, with no noticeable effect on the splitting of the two boundary currents. This suggests that the results of the relative vorticity compensation are generally correct despite the closure problem. Higher resolution or better boundary fitting are needed in order to balance the PV budget.
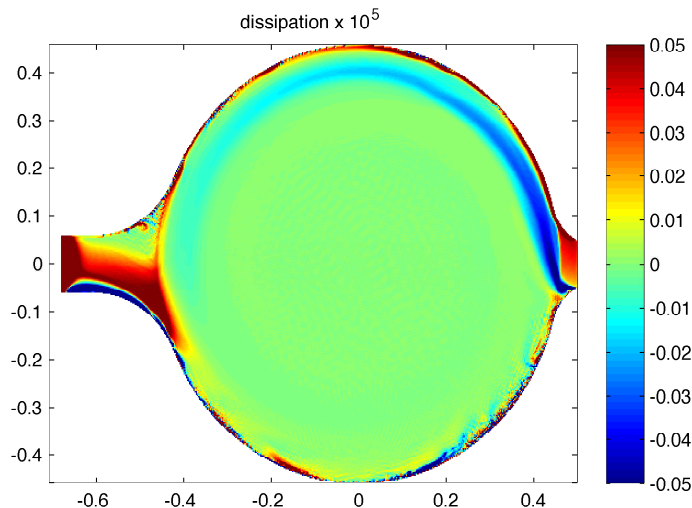

Figure 15: Typical spatial dissipation $(-\lambda \nabla \times (u/h))$ for a simulation with side inflow.

4 Conclusions and further work

We have performed experiments and numerical simulations to investigate the basin circulation upstream of a hydraulically controlled sill. Previous work by Yang (2005) and Pratt (1997) has shown a simple dependence of the direction of circulation in the basin on the relative thickness of the inflow and outflow. This relationship is based on the assumption of negligible relative vorticity at the basin openings, compared with the component of planetary vorticity in the fluid. Previous numerical studies have enforced this assumption by constraining the direction and transport of the flow through the openings. We have shown in a series of experiments and numerical simulations that, for the parameter range examined here, the relative vorticity may be significant if the flow is given freedom to adjust. Changes in outflow thickness may be compensated by changes in relative vorticity, rather than changes in dissipation brought about by a reversed circulation.

Repeating the analysis of the relative vorticity contribution to the PV budget in additional numerical simulations with an extended parameter range (in particular, increasing f, so that the Rossby radius is a fraction of the strait width) would enable the results to be more readily applied to the ocean. Further work on the PV balance would also require

closure of the budget by increasing the resolution of the simulations or using improved boundary fitting.

A further extension of this work would be to compare the response of the PV balance in flows with subcritical and critical outflows. It is possible that the significant changes in relative vorticity we have observed are a feature of the hydraulic flows and would not be present in the subcritical case.

5   Acknowledgements

References

[1] T. ELDEVIK, J. E. NILSEN, D. IOVINO, K. A. OLSSON, A. B. SANDO, AND H. DRANGE, *Observed sources and variability of Nordic seas overflow*, Nature Geoscience, (2009).

[2] A. KOHL, *Variable source regions of Denmark Strait and Faroe Bank Channel overflow waters*, Tellus Series A-Dynamic Meteorology and Oceanography, (2010).

[3] B. HANSEN, W. R. TURREL, AND S. OSTERHUS, *Decreasing overflow from the Nordic seas into the Atlantic Ocean through the Faroe Bank Channel since 1950*, Science, (2001).

[4] J. B. GIRTON, L. J. PRATT, D. A. SUTHERLAND, AND J. F. PRICE, *Is the Faroe Bank Channel overflow hydraulically controlled?*, Journal of Physical Oceanography, (2006).

[5] A. NIKOLOPOULOS, B. K., H. R., AND P. A. LUNDBERG, *Hydraulic estimates of Denmark Strait overflow*, Journal of Geophysical Research-Oceans, (2003).

[6] A. E. GILL, *The hydraulics of rotating-channel flow*, Journal of Fluid Mechanics, (1977).

[7] K. R. HELFRICH AND L. J. PRATT, *Rotating hydraulics and upstream basin circulation*, Journal of Physical Oceanography, (2003).

[8] L. PRATT, *Hydraulically drained flows in rotating basins. Part II: Steady flow*, Journal of Physical Oceanography, (1997).

[9] J. YANG, *The Arctic and subarctic ocean flux of potential vorticity and the Arctic ocean circulation*, Journal of Physical Oceanography, (2005).

[10] J. YANG AND J. F. PRICE, *Water-mass formation and potential vorticity balance in an abyssal ocean circulation*, Journal of Marine Research, (2000).

[11] J. A. WHITEHEAD AND J. SALZIG, *Rotating channel flow: control and upstream currents*, Geophysical and astrophysical fluid dynamics, (2001).

[12] K. HELFRICH, A. KUO, AND L. PRATT, *Nonlinear rossby adjustment in a channel*, Journal of Fluid Mechanics, 390 (1999), pp. 187–222.